

Article

The C/N Ratio's Effect on a Membrane-Aerated Biofilm Reactor (MABR): COD and Nitrogen Removal, Biofilm Characteristics, and Microbial Community Structure

Huiyun Zhong ¹, Liangfei Dong ^{1,*}, Yuanyuan Tang ², Lin Qi ² and Mengyu Wang ²¹ School of Urban Construction, Changzhou University, Changzhou 213164, China² School of Environmental Science and Engineering, Changzhou University, Changzhou 213164, China

* Correspondence: dlf@cczu.edu.cn

Abstract: In this study, a laboratory-scale membrane aerated biofilm reactor system was operated successively through four phases with different C/N ratios (7, 5, 3, and 1) for 15 days each to investigate the C/N ratio's effect on the COD and nitrogen removal. The COD and NH_4^+ -N removal efficiencies were slightly affected; however, NO_3^- -N accumulated in the C/N = 1 phase, and slight NO_2^- -N accumulation was observed in the C/N = 7 phase, leading to lower total nitrogen (TN) removal in the two phases. The TN removal efficiency reached the highest in the C/N = 5 phase at around 70%, and the TN concentration was reduced to 12.3 mg/L on average. Biomass and biofilm thickness had a positive correlation with C/N ratios. The C/N ratio affected not only the generation of extracellular polymeric substances but also their chemical composition. Microbial analysis revealed that a C/N ratio of 5 was the most suitable for both nitrifying and denitrifying bacteria, and a higher C/N ratio favored aerobic denitrifying microbes.

Keywords: C/N ratio; COD removal; nitrogen removal; MABR

Citation: Zhong, H.; Dong, L.; Tang, Y.; Qi, L.; Wang, M. The C/N Ratio's Effect on a Membrane-Aerated Biofilm Reactor (MABR): COD and Nitrogen Removal, Biofilm Characteristics, and Microbial Community Structure. *Water* **2023**, *15*, 4298. <https://doi.org/10.3390/w15244298>

Academic Editor: Jesus Gonzalez-Lopez

Received: 17 November 2023

Revised: 11 December 2023

Accepted: 14 December 2023

Published: 17 December 2023



Copyright: © 2023 by the authors. Licensee MDPI, Basel, Switzerland. This article is an open access article distributed under the terms and conditions of the Creative Commons Attribution (CC BY) license (<https://creativecommons.org/licenses/by/4.0/>).

1. Introduction

Water is an essential factor for both development and sustainability, which is a challenge due to its scarcity since the beginning of the 21st century [1,2]. Wastewater treatment and recycling continue to be important methods to relieve the pressure of water scarcity. Researchers have been dedicated to developing and adapting innovative energy-saving and economic wastewater treatment technologies to support ecological system health and sustained social stability [1,3–6]. Among these novel water and wastewater treatment technologies, the membrane biofilm reactor (MBfR) has attracted attention due to the special counter-diffusion of the electron donor and acceptor [7–9]. MBfRs use hydrophobic gas-permeable membranes to deliver gases into the biofilm attached to the membrane's surfaces, while the substrates from bulk liquid penetrate the biofilm from the opposite side [9,10]. Particularly, when oxygen is supplied from the membrane lumen, a membrane-aerated biofilm reactor (MABR) is then developed. An inner oxygen-rich zone and outer oxygen-depleted zone are created in the attached membrane-aerated biofilm (MAB), where a diverse range of microorganisms are present to accomplish complex microbial functions.

MABR features the counter-diffusion model, where oxygen and substrates disperse into the biofilm from opposite directions [11,12]. Therefore, the oxygen level is the highest at the interface of the membrane and the biofilm attached. As the oxygen penetrates the biofilm, it is consumed by microbes such as ammonia-oxidizing bacteria (AOB) and nitrite-oxidizing bacteria (NOB). Therefore, the oxygen level at the biofilm and bulk liquid interface could become very low or potentially zero. Based on MABR's counter-diffusion property, it shows advantages over other conventional wastewater treatment methods, including high oxygen transfer rates (OTRs), up to 100% oxygen transfer efficiency (OTE) [13,14], one-stage simultaneous nitrification and denitrification (SND) [15,16], partial nitrification and

anammox (PN/A) [13,17], etc. Compared to other biofilm reactors, MABR could achieve a remarkably high nitrification rate (NR), resulting from high OTRs [18,19].

SND is an ideal nitrogen removal process as it effectively and economically reduces energy consumption and simplifies operation [20]. Nitrogen removal in the activated sludge process is influenced by the C/N ratio, and a high C/N ratio (8 or even higher) is essential for the SND process because denitrifying heterotrophic bacteria consume biodegradable organics as electron donors [21]. Therefore, the C/N ratio in municipal wastewater is an important parameter to be considered. Generally, the C/N ratio in municipal wastewater is low for biological treatment for both COD and nitrogen removal, so exogenous carbon sources, commonly sodium acetate, are dosed, increasing operation costs [22,23]. Otherwise, excessive nitrogen discharged into natural water would result in eutrophication, causing risks to ecology and, eventually, human health through the food chain [24]. In the MABR system, sufficient SND could be achieved at lower C/N ratios due to the stratified biofilm and high OTR, which makes it superior in saving operation costs (less or even no exogenous carbon sources and low aeration consumption) [25]. Yet, in China, the C/N ratio in municipal wastewater is even lower due to living habits and no diversion of rain and sewage water in certain areas [26]. As a result, MABR is more likely to reach SND in municipal wastewater treatment plants in China. However, there are few studies concerning the nitrogen removal performance in the MABR system at low C/N ratios. This study focuses on the effect of C/N ratios on MABR treatment performance and would provide both theoretical and technical support for MABR application in different situations.

2. Materials and Methods

2.1. MABR System Set-Up and Operation

The lab-scale MABR system was designed and set up as shown in Figure S1. The reactor was rectangular with a volume of 5 L and operated with a hydraulic retention time (HRT) of 24 h. An air blower (Baihui Blower Co. Ltd., Jinan, China) was used to supply air through the porous hydrophobic polytetrafluoroethylene hollow fiber membrane module (Nanjing Bidun Environmental Protection Technology Inc., Nanjing, China) with a length of 40 cm and a membrane square of 0.1 m². The outside and inside diameters of the fibers were 1 and 0.5 mm, respectively. The air-feeding pressure was monitored by connecting one end of the fibers to an air-flow meter with the other end sealed. The reactor was covered with aluminium foil to eliminate light exposure. The system was operated at room temperature (25 ± 2 °C), and the air supply pressure was set at 10 Kpa.

To start the MABR system, the reactor was seeded with return-activated sludge from the secondary clarifier in a wastewater treatment plant in Changzhou City, China. The MLSS and MLVSS of the sludge were 6740 mg/L and 4250 mg/L, so the calculated MLVSS/MLSS ratio was 63.05%. A sludge concentration of 3500 mg VSS/L was achieved by adding synthetic wastewater to reach a 4 L solution volume. The composition of the synthetic wastewater was determined according to previous study [24] as (mg/L): glucose 260, peptone 260, (NH₄)₂SO₄ 236, KH₂PO₄ 34, K₂SO₄ 105, MgSO₄·7H₂O 55, NaCl 45, NaHCO₃ 90, and Na₂CO₃ 450. The dissolved oxygen (DO) concentration was maintained at 1.5~2.5 mg/L, and glucose, (NH₄)₂SO₄, and KH₂PO₄ were added per 24 h to provide adequate nutrients for sludge attachment to the membrane. All the chemicals used in this study were supplied by Merck Chemicals (Shanghai) Co., Ltd. After 7 days, the reactor was switched to continuous feeding mode at a speed of 0.01 m/s with an HRT of 24 h for 30 days for biofilm formation.

The reactor was maintained for 20 days until it reached a stable state. Then, the reactor was operated through 4 phases with different C/N ratios (7, 5, 3, and 1) successively at an HRT of 24 h (Table 1), and each phase lasted 15 days before switching to a lower C/N ratio. Thus, the organic loading rate (OLR) was steadily maintained at 0.56 kg COD/m³/d, 0.42 kg COD/m³/d, 0.24 kg COD/m³/d, and 0.08 kg COD/m³/d in C/N = 7, 5, 3, and 1 phases, respectively.

Table 1. MABR operation through 4 phases with different C/N ratios.

Parameter (mg/L)	Phase (15 Days/Phase)			
	C/N = 7	C/N = 5	C/N = 3	C/N = 1
COD	560 ± 5	420 ± 5	240 ± 5	80 ± 5
NH ₄ ⁺ -N	50 ± 5	50 ± 5	50 ± 5	50 ± 5
TN	80 ± 5	80 ± 5	80 ± 5	80 ± 5

2.2. Chemical Analysis

Triplicate liquid samples were taken regularly for chemical analysis with syringes and then filtered by 0.22 µm PES filters (Merck Millipore Ltd., Shanghai, China) before being stored in a 4 °C fridge. Nitrogen species, including NH₄⁺-N, NO₃⁻-N, NO₂⁻-N, and total nitrogen (TN), were determined following APHA methods [27]. The samples were digested using Hach digestion vials, and the COD level was determined by a Hach spectrophotometer (Hach, New York, NY, USA).

2.3. Biofilm Analysis

Membranes with biofilms of the same length (50 mm) were cut by a sterilized scissor in different operation phases to quantify the biomass adhered through weight measurement. Each time, three randomly selected pieces of the membrane were cut and analyzed to obtain triplicate results. After the cut, both ends of the residue membrane in the reactor were sealed by resin adhesive to prevent air blow. Before measurement, a circular filter paper was dried to constant weight and weighed with a dried weighing bottle as Weight A. The sampled piece of the membrane was immersed in 20% NaOH for 12 h and then sonicated for biofilm to peel from the membrane surface into a liquid phase, which was then filtered by the dried filter paper to sample the biomass. Then, the filter paper with biomass was dried to constant weight and placed in the weighing bottle as Weight B. The surface area of the sampled membrane was calculated and marked as *a*. The amount of biomass was calculated as $Biomass = (B - A)/a$.

Biofilm thickness was measured according to Celmer's method [28]. The membrane module was removed from the reactor for 15 min to allow the water to drain. Then, the biofilm from a certain field of the module was removed with a sterilized plastic scraper to a partially deionized water-filled plastic syringe, and then the volume increase in the liquid in the syringe was the biomass volume. So, biofilm thickness could be calculated as:

$$T = \sqrt{\frac{V}{l\pi} + R^2} - R, \quad (1)$$

where *T* is the biofilm thickness, *V* is the biomass volume, *l* is the length of the selected membrane fiber, and *R* is the fiber radius.

Biofilm morphology was observed by a scanning electron microscope (SEM, HITACHI SU3500, Hitachi High-Tech Corp., Tokyo, Japan) at 15 kV accelerating voltage. A piece of membrane fiber with biofilm on the surface was cut and immediately fixed by 2.5% glutaraldehyde for 4 h. Then, the fiber was dehydrated by a gradient of ethanol (20%, 50%, 70%, and 100% vol/vol) and dried under nitrogen gas blow. Before observation, the fiber was coated with a thin gold film.

2.4. Extracellular Polymeric Substances (EPS) Extraction and Analysis

Centrifugation, ultrasonication, and heating are the most applied methods to extract EPS [29]. In this study, EPS was extracted based on the heating method described in a previous study [30]. The procedure was as follows: for each test, three pieces of 5 cm long hollow fiber membrane uniformly covered with biofilms were cut and washed three times with deionized water in a sterile bottle. The biofilm was stripped using a sterile scalpel to 20 mL deionized water and heated for 29 min (80 °C) in water bath. Finally, the EPS solution was centrifuged at 5000 rpm for 15 min and the supernatant was filtered by

0.45 µm membrane. The polysaccharides (PS) in the EPS extracts were detected by anthrone assay (BPA) [31], using glucose to calibrate. The proteins (PN) in the EPS extracts were determined by the Coomassie brilliant blue G-250 dye-binding method, according to Pierce and Suelter [32]. The sum of the PS and PN contents expressed the total amount of EPS.

Three-dimensional fluorescence spectroscopy (3D-EEM) has been widely applied to the study of various substances in EPS. A 3D fluorescence spectrometer (Cary Eclipse, Agilent, Palo Alto, Cal., USA) was used to analyze the EPS characteristics of the biofilms during different C/N phases in the reactor. The EPS solution was diluted with deionized water to the appropriate concentration to ensure correct and accurate detection. Using ultrapure water as the blank, the EPS solution was analyzed at the excitation wavelength (Ex) of 220~450 nm by 5 nm step and emission wavelength of 280~550 nm by 1 nm step, and the slit width between the two wavelengths was set as 5 nm, at a photomultiplier voltage of 700 V and a scanning speed of 2400 nm/min. The spectra data were analyzed using Surfer 12.0 software (Golden Software, Golden, Colorado, USA).

An infrared spectrometer (Nicolet-460, Thermo Fisher Scientific Inc., Waltham, MA, USA) was used to obtain the Fourier transform infrared spectra for main functional groups analysis in EPS to characterize the molecular structure. The EPS solution was freeze-dried for 48 h, crushed into powder, mixed well with KBr (1:100), pressed into a translucent sheet, and then analyzed at 400~4000/cm.

2.5. DNA Extraction and Analysis

Biofilms in different C/N phases were sampled and stored in a −80 °C freezer. The DNA of microbes was extracted using the E.Z.N. ATM Mag-Bind Soil DNA Kit (OMEGA bio-tek, Norcross, GA, USA), and the concentration was determined by the Qubit dsDNA HS Kit (Thermo Fisher, Scientific Inc., Waltham, MA, USA). Primers 341F (5'-CCTACGGGGGNGGCWGCAG-3') and 805R (5'-GACTACHVGGGGTATCTAATCC-3') were used to amplify the highly variable region V 3~V 4 of the 16S r RNA genes. Polymerase chain reaction (PCR) was performed using the PCR device (ETC811, Beijing Dongsheng Innovation Biotechnology Co., Beijing, China). Sequencing was performed using IlluminaMiSeq (Bioengineering (Shanghai) Co., Shanghai, China). The Chao and ACE indices were used to illustrate the abundance of the microbial community, while the Shannon, Simpson, and Coverage indices were used to evaluate microbial diversity [33].

3. Results and Discussion

3.1. Reactor Performance

3.1.1. Batch Tests

The reactor was maintained at each C/N ratio for 15 days with an HRT of 24 h by replacing the medium in the reactor with the synthetic wastewater daily, and the water quality was measured every hour during one HRT cycle during batch tests. The results of the last three cycles were recorded in triplicate and are shown in Figure 1.

As shown in Figure 1a, COD in the feeding medium varies for different C/N ratio experiments but could decrease towards 0 after 7 h. The decreasing rate in the C/N = 7 phase during the first hour was the highest (approximately 330 mg/(L·h)) of the HRT cycle. Figure 1b shows that the NH₄⁺-N removal efficiencies of C/N ratios 1, 3, and 5 were similar, while they were lower with C/N ratio 7, indicating suppressed ammonium oxidation. Combined with Figure 1f, DO decreased dramatically during the first hour under all C/N ratio conditions, but it decreased to approximately 1.3 mg/L in C/N = 1 phase, while DO was consumed completely during the first hour in the other three phases. DO gradually increased to 3 mg/L after 9 h in the C/N = 1 phase, while it remained at 0 and started to increase after 7 hours of operation and gradually reached a stable level at slightly above 1 mg/L in the C/N = 3 phase. DO started to show an increasing trend at hour 12 and increased to approximately 2 mg/L at hour 24 in the C/N = 5 phase. On the contrary, it remained at 0 until hour 24 in the C/N = 7 phase. Combined with the results in Figure 1a,b,f, DO could be the limiting parameter for NH₄⁺-N removal in the C/N = 7

phase, as the aerobic heterotrophic bacteria competed with ammonia-oxidizing bacteria (AOB) for oxygen to remove the high COD.

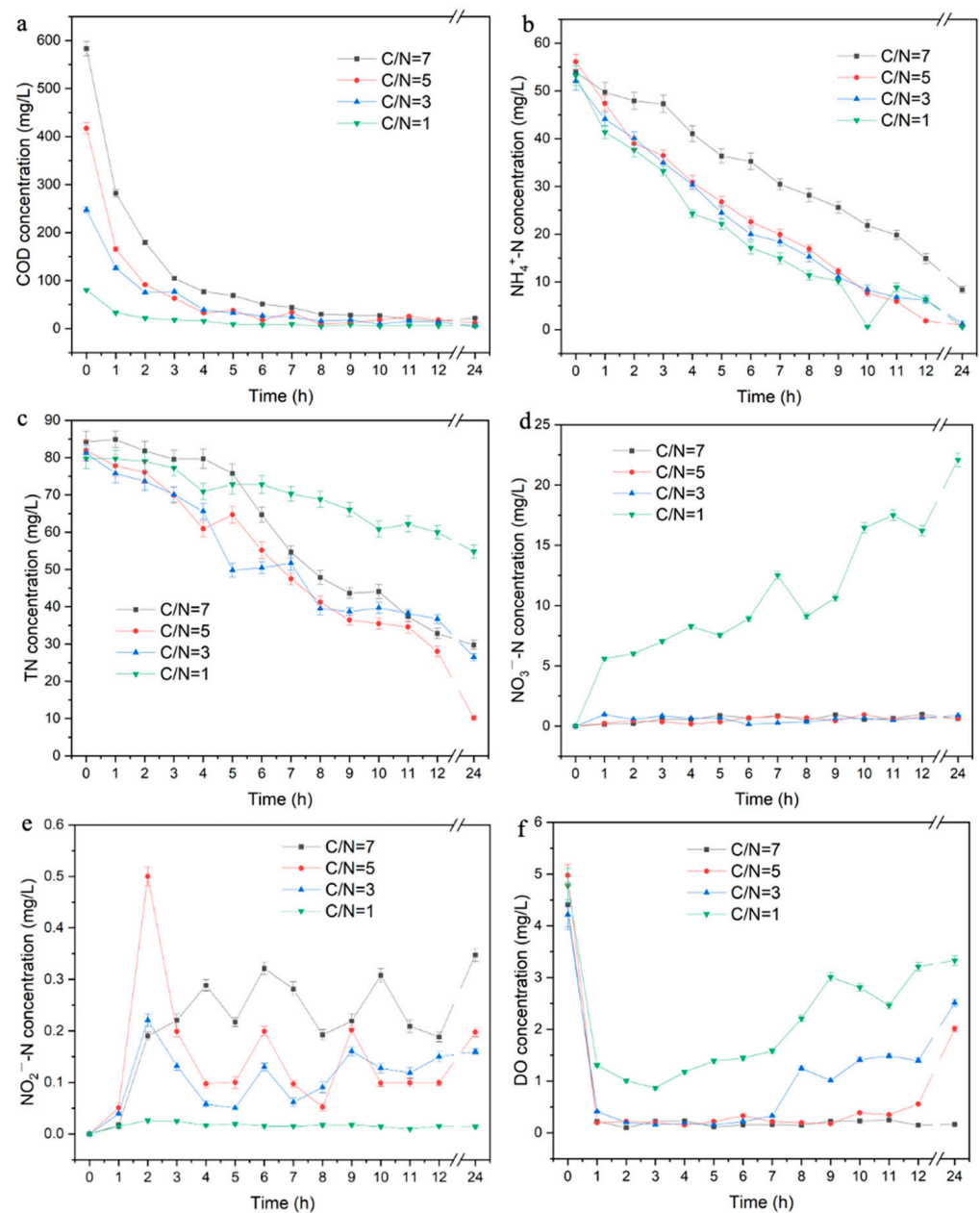


Figure 1. Water quality of the batch tests under different C/N ratio conditions ((a) COD; (b) $\text{NH}_4^+\text{-N}$; (c) TN; (d) $\text{NO}_3^-\text{-N}$; (e) $\text{NO}_2^-\text{-N}$; (f) DO).

In the C/N = 3, 5, and 7 phases, $\text{NO}_3^-\text{-N}$ stayed at around 0 (Figure 1d) in the cycle, but $\text{NO}_2^-\text{-N}$ accumulated (Figure 1e), indicating a depressed nitrite-oxidizing process, which could be attributed to oxygen limitation (Figure 1f); in contrast, $\text{NO}_3^-\text{-N}$ and $\text{NO}_2^-\text{-N}$ showed opposite profiles in the C/N = 1 phase. Accordingly, total nitrogen (TN) removal efficiency showed similar trends in the C/N = 3, 5, and 7 phases, while it decreased after 4 h in the cycle of the C/N = 1 phase, which could be due to the aerobic conditions in the phase, depressing the nitrate-reducing activity (Figure 2d,f).

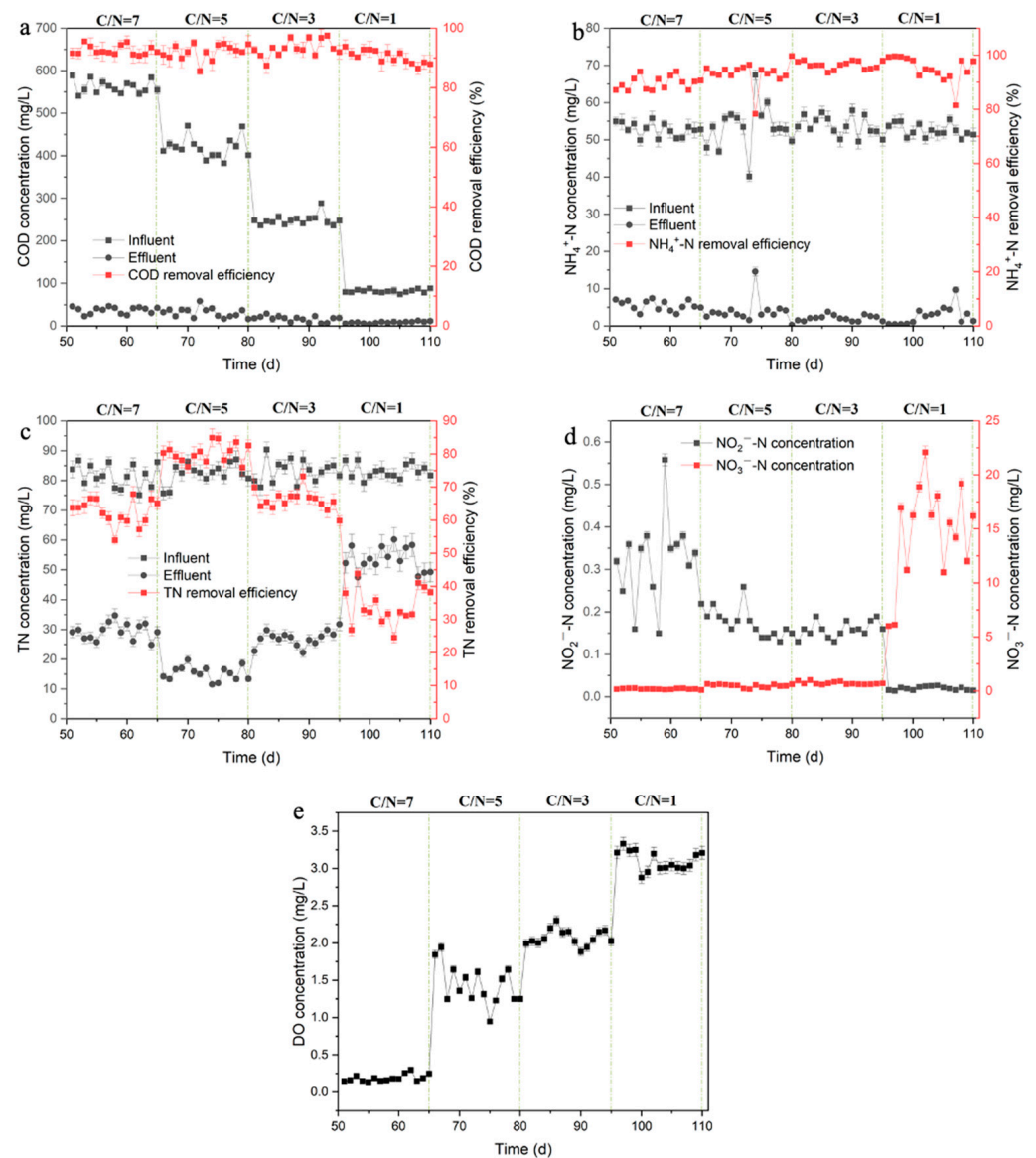


Figure 2. Water quality of the long-term continuous feeding tests under different C/N ratio conditions ((a) COD; (b) NH₄⁺-N; (c) TN; (d) NO₃⁻-N and NO₂⁻-N; (e) DO).

3.1.2. Long-Term Continuous Feeding Tests

The reactor was switched to continuous mode with an HRT of 24 h and maintained at each C/N ratio for 15 days, with the water quality in both influent and effluent measured every day and the removal efficiency calculated by $(Con_{inf} - Con_{eff})/Con_{inf} \times 100\%$.

Although COD levels in the feeding synthetic wastewater varied in different C/N phases, COD removal efficiency showed a similar profile in all phases at approximately 90~95%, indicating the aerobic heterotrophic bacteria's high activity in the reactor. The high oxygen consumption resulted in lower DO levels in the reactor in higher C/N phases (Figure 2e). NH₄⁺-N removal efficiency in all phases showed a stable transition between 89% and 96% (Figure 2b), indicating the high ammonia-oxidizing activity of the biofilm.

As shown in Figure 2d, reconciled with batch tests, NO₃⁻-N concentration was scarce in the C/N = 3, 5, and 7 phases and started to accumulate in the C/N = 1 phase at approximately 15 mg/L with fluctuation. In the C/N = 7 phase, NO₂⁻-N showed an unstable profile with an average accumulation of 0.3 mg/L. NO₂⁻-N concentration remained relatively stable at approximately 0.15 mg/L in the C/N = 3 and 5 phases, while it was 0 in the C/N = 1 phase. Correspondingly, the C/N = 1 phase had the lowest TN removal efficiency

(around 35%), and the C/N = 5 phase had the highest (approximately 70%), with C/N = 3 and 7 at roughly 55% in Figure 2c. The drop in TN removal with the decreasing C/N ratio was also reported in previous studies, which could be attributed to the insufficient carbon source for denitrifiers [34,35].

3.2. Biofilm Characteristics

3.2.1. Biomass Density and Thickness of Biofilm

Biomass density and the thickness of the biofilm are important parameters to evaluate the active biomass, which reflects the growth of the microbes in the reactor. In Figure 3, biomass density and biofilm thickness had a positive correlation and decreased along with the decrease in C/N ratios in the reactor. Biomass density was only 16.32 g/m² in the C/N = 1 phase, which could be because lower COD hindered heterotrophic microbes' growth and affected nitrogen removal as nitrite/nitrate-reducing bacteria are heterotrophic. Combined with Figure 2, the TN removal rate could be calculated per biomass weight per membrane surface area as 1.65, 2.20, 2.07, and 1.22 mg N/g biomass/m² in the C/N = 1, 3, 5, and 7 phases, respectively. The TN removal rate was the highest in the C/N = 3 phase, indicating a high nitrogen removal capacity at a lower C/N ratio in the MABR system.

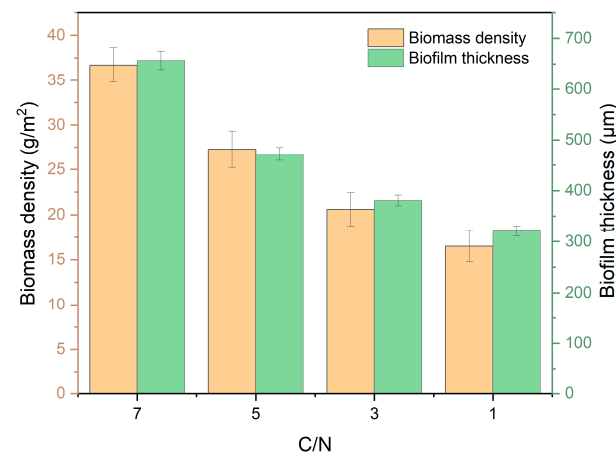


Figure 3. Biomass density and biofilm thickness under different C/N ratios.

3.2.2. EPS Content and Composition

The amount and components of EPS in the MABR system under different C/N conditions are shown in Figure 4a. From phase C/N = 7 to C/N = 1, the content of PS in the EPS decreased from 29.31 mg/g VSS to 5.13 mg/g VSS, and the content of PN decreased from 96.83 mg/g VSS to 20.53 mg/g VSS. Correspondingly, the PN/PS ratio slightly increased from 3.30 to 4.00, indicating that the C/N ratio had a greater effect on the production of PS in the EPS. As COD concentration was set lower to achieve a low C/N ratio (i.e., insufficient carbon source) in this study, the carbon source was prioritized for microbial growth rather than PS synthesis, leading to an increasing PN/PS ratio. When the C/N was high, the microorganisms tended to utilize the organic carbon source to increase the synthesis of ATP, which led to the production of PS and thus favored the production of EPS. However, when the C/N was low, the lack of a sufficient carbon source led to the obstruction of microbial growth and products, and the EPS production decreased. Moreover, under starvation, PS and PN in EPS can be used as energy for cellular metabolism and are utilized by microorganisms, leading to PS and PN decomposition in low C/N phases. Overall, C/N had a significant effect on the generation and composition of EPS in the MABR system, and the PS and PN contents in the EPS decreased to a certain extent when C/N was decreased. As the most important component of biofilm, EPS accounted for 50~80% of the total mass, and the total EPS content in the system was reconciled with the profiles of biomass and biofilm thickness in Figure 4a. In addition, the content of PN was significantly higher than that of PS, indicating that PN has a great influence on the formation of biofilm.

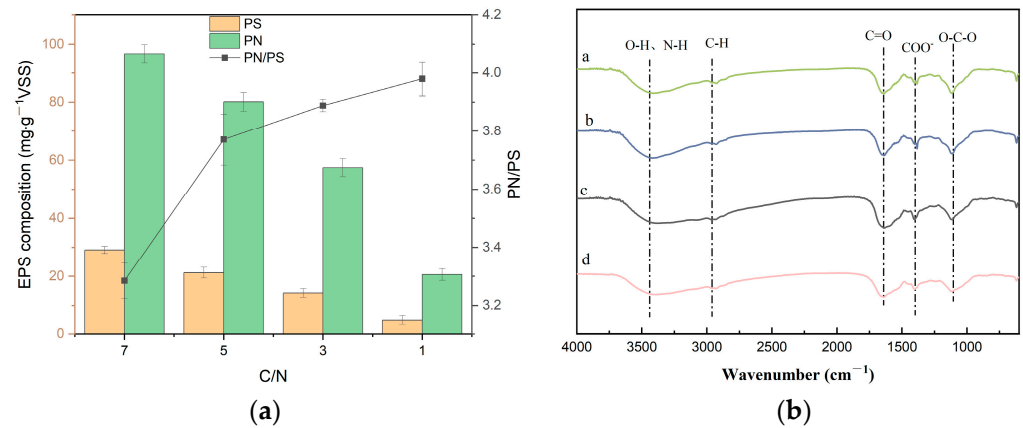


Figure 4. EPS composition and content under different C/N ratios as in (a) and infrared spectrum of MABR system internal EPS under different C/N ratios (a—C/N = 7; b—C/N = 5; c—C/N = 3; d—C/N = 1) as in (b).

In Figure 4b, the FTIR spectra of EPS in different C/N phases show that there were absorption peaks at 3410~3440/cm, which were caused by the O-H or amino group stretching vibration. Around 1650/cm, an adsorption peak appeared due to the elastic vibration of C=O. The peak around 1007/cm could be attributed to the C-O stretching vibration of polysaccharides and lipids. Based on the FTIR results, EPS contained proteins, polysaccharides, lipids, and polymers.

Under different C/N conditions, four fluorescence peaks marked as A, B, C, and D were observed in the EPS in Figure 5. Peak A (Ex/Em 270~280/280~350 nm) represented the microbial metabolites, the main component of which is a protein derivative (the amino acid tryptophan) that is often detected in EPS [36]. Among them, B and C were humic acids, which were detected at Ex/Em 350/400~450 nm and Ex/Em 280/430~450 nm, respectively, and peak D (Ex/Em 220~230/280~350 nm) represents aromatic protein substances.

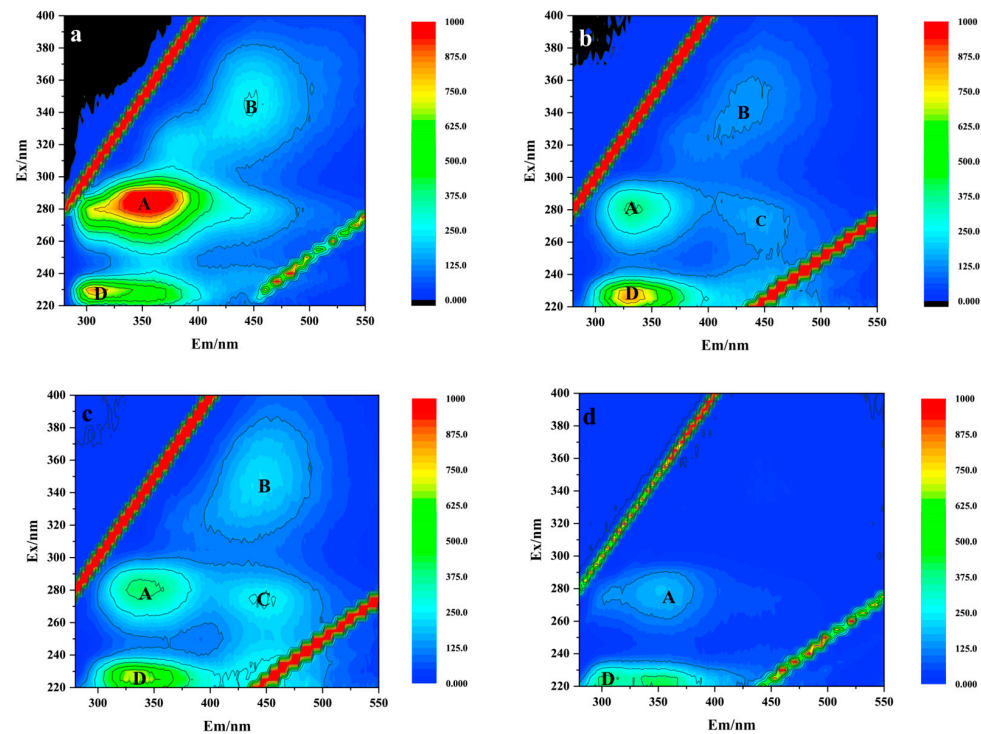


Figure 5. Three-dimensional fluorescence diagram of biofilm EPS under different C/N ratios ((a) C/N = 7; (b) C/N = 5; (c) C/N = 3; (d) C/N = 1).

The intensities of A and B fluorescence peaks weakened with the decrease in C/N, and B and C peaks disappeared under the condition of C/N = 1, which may be related to the utilization of EPS by the microorganisms' growth and metabolism. In the absence of a carbon source, microorganisms utilize cell-stored energy and regulate their metabolic pathways to sustain their normal growth and metabolism [37]. This could explain that when C/N decreased, the biomass of the system decreased significantly, leading to the degradation of EPS organisms. Peak D showed strong fluorescence at C/N of 5, 3, and 1, suggesting relatively high PN production. The above results indicated that in the MABR system, the C/N ratio not only affected the generation of EPS but also the chemical composition of EPS.

3.2.3. Biofilm Morphology

In Figure 6, the biofilms on hollow fiber membrane surfaces in different C/N phases were observed by SEM. Figure 6a showed a large number of microbes in strongly tied clusters on the membrane surface in the C/N = 7 phase, indicating a mature biofilm structure with abundant EPS. In the C/N = 5 phase, the biofilm structure was relatively loose compared to the C/N = 7 phase, with debris probably from microbes' lysis. The structure started to become uneven and unsmooth along with the C/N ratio decreasing, and phase filamentous bacteria accumulated in C/N = 1, which would be due to the lack of carbon source.

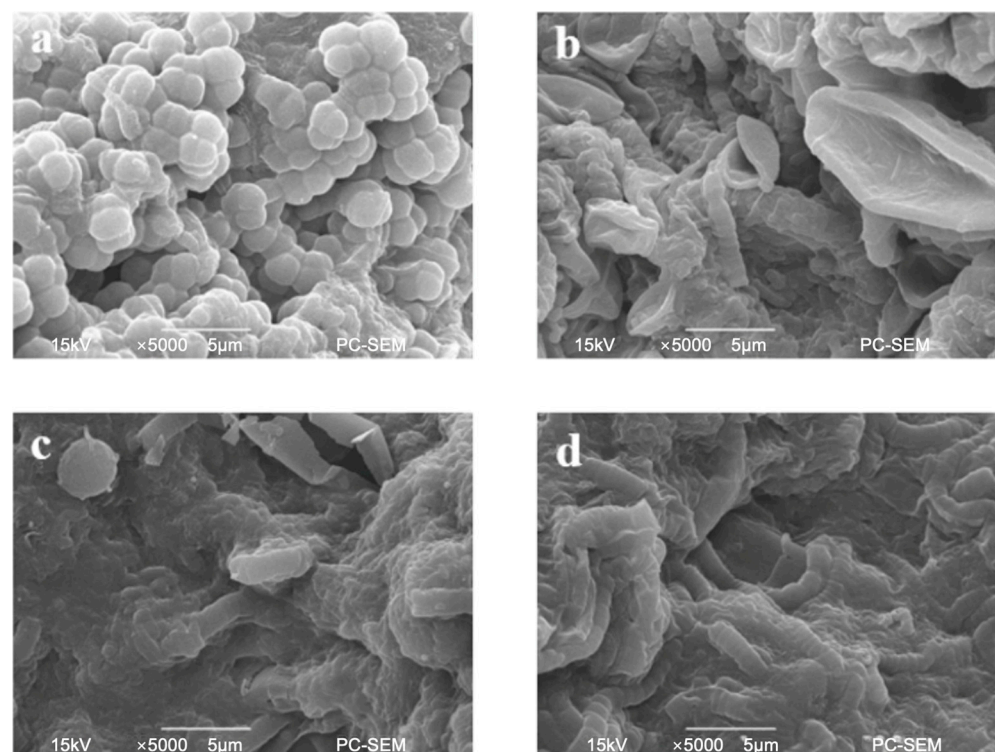


Figure 6. SEM images of biofilms under different C/N ratios ((a) C/N = 7; (b) C/N = 5; (c) C/N = 3; (d) C/N = 1).

3.3. Microbial Community Structure

3.3.1. Microbial Diversity

As shown in Table 2, 37,857, 38,478, 33,701, and 40,247 valid sequences were obtained for biofilm samples in the C/N = 1, 3, 5, and 7 phases, respectively. They can be clustered into 584, 603, 656, and 597 OTUs at a 97% similarity level. The results showed that the number of OTUs increased with the C/N increase, which decreased in the C/N = 7 phase. The sequencing depth (coverage) of all four samples was greater than 99.7%, indicating that the sequencing depth covered the whole microbial community structure information. The

Chao1 and ACE indices increased the highest in the C/N = 5 phase before starting to decrease in the C/N = 7 phase, which indicated that the abundance of microbial communities in the MABR system reached the highest level in the C/N = 5 phase. The Shannon index reached its highest at 4.66 in the C/N = 1 phase, and the Simpson index decreased from 0.033 to 0.022, with the C/N ratio switching from 7 to 1 gradually, indicating an increasing microbial diversity along with the C/N ratio decreasing. Therefore, the C/N ratio had a great influence on the structure of the bacterial community in the MABR reactor.

Table 2. Microbial community α diversity index.

Sample No.	C/N Ratio	Sequences Number	OTUs	Shannon	Simpson	Chao1	ACE	Coverage
C-1	1	37,857	584	4.66	0.022	643.5	637.87	0.998
C-2	3	38,478	603	4.58	0.026	669	660.03	0.998
C-3	5	33,701	656	4.59	0.027	745.79	742.91	0.997
C-4	7	40,247	597	4.42	0.033	660.2	646.78	0.998

The similarity of the microbial community in different C/N phases was illustrated and analyzed by dilution curve, Venn diagram, principal component analysis, and cluster analysis (Figure 7). When the number of sequences exceeded 10,000, the dilution curve tended to be flat, indicating that the sequencing could truly reflect the diversity of microbial communities in the samples [38]. In Figure 7b, the number of shared OTUs by all four samples was 322, and the number of independent OTUs was 207, indicating that a small number of unique bacteria existed in different C/N conditions. Principal component analysis (PCA) was performed by dimensionality reduction, replacing multiple variables with a few. PCA analysis could reduce the number of dimensions in the factor analysis, replacing multiple variables with a few to portray the variability among samples [39]. PC1 and PC2 represented 70.67% and 23.96% of the variables, respectively. Two samples, C-1 and C-2, were closer to each other, representing the microbial communities in C/N = 1 and 3 were more similar. The other two samples were spread much more dividedly, indicating that their community structures varied. The Bray–Curtis similarity distance algorithm was used to analyze the clustering of the different groups (Figure 7d). The results were consistent with the PCA analysis, which verified that the microbial communities under different C/N conditions had different evolution patterns.

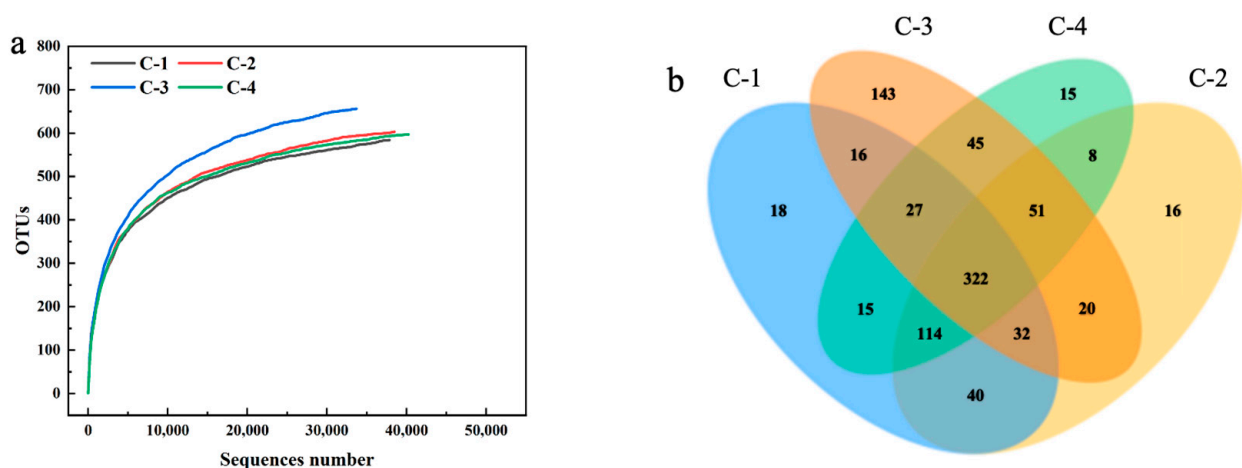


Figure 7. Cont.

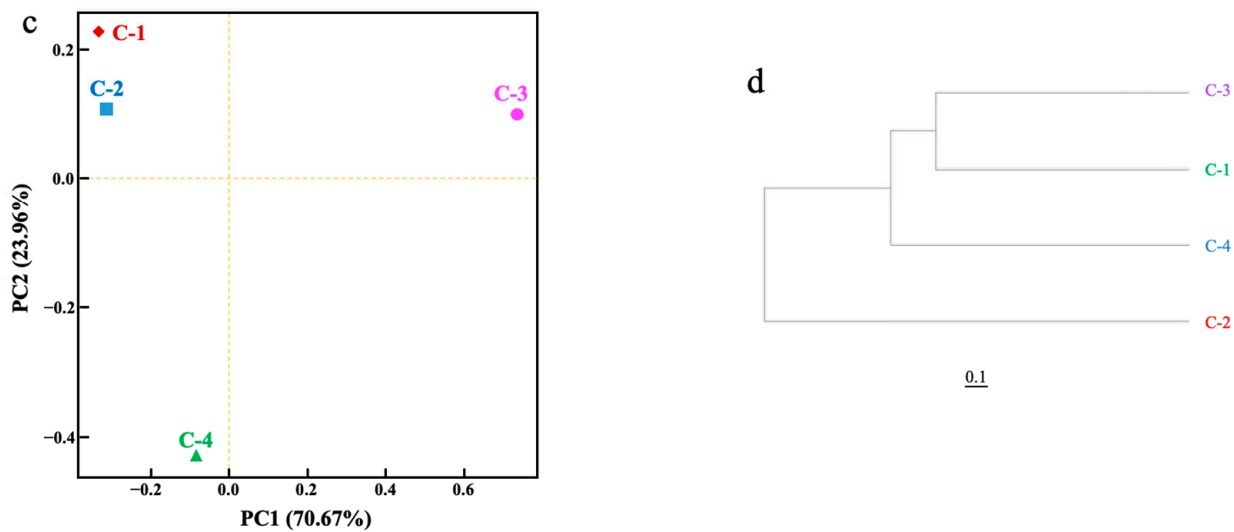


Figure 7. Similarity of microbial community under different C/N ratios ((a) dilution curve; (b) Venn diagram; (c) principal component analysis; (d) cluster analysis).

3.3.2. Microbial Community Analysis

The microbial community structure of microorganisms at phylum, class, family, and genus levels in the MABR system under different C/N conditions is shown in Figure 8. Among the known bacterial species, 13 species have been identified with abundance >1%, including *Proteobacteria* (35.94~50.73%), *Chloroflexi* (3.23~9.38%), *Firmicutes* (0.63~13.57%), *Candidatus Saccharibacteria* (0.96~6.16%), *Planctomycetes* (1.82~5.37%), *Spirochaetae* (0.35~6.15%), *Acidobacteria* (0.6~1.9%), *Bacteroidetes* (8.49~26.61%), *Actinobacteria* (0.90~1.56%), *Gemmatimonadetes* (1.13~1.20%), *Verrucomicrobia* (0.56~2.22%), and *Nitrospirae* (0.012~1.29%). As the dominant microorganisms in the municipal wastewater treatment system [40], the abundance of *Proteobacteria* remained stable during all the phases in the MABR system. The relative abundance of *Proteobacteria* was the highest in the C/N = 5 phase, and it was similar during the other three phases, which was closely related to the removal of TN in the influent water. On the contrary, the relative abundance of *Bacteroidetes* was the lowest in the C/N = 5 phase, indicating that this was the most unfavorable condition for the growth of *Bacteroidetes*, which was the main bacteria for organic matter degradation. The abundance of *Chloroflexi* had a negative correlation with C/N ratios, and in particular, it reached 9.38% in the C/N = 1 phase, implying a lower C/N ratio favored their growth. As *Chloroflexi* belonged to the filamentous bacteria, its increasing abundance in lower C/N ratio conditions was also reconciled with the SEM visualization in Figure 6.

As shown in Figure 8b, the composition of the microbial community at the level of class under different C/N conditions was generated. *β-Betaproteobacteria* and *Sphingobacteria* were the major classes in the *Proteobacteria* phylum. *β-Betaproteobacteria* was the most dominant class, and its abundance was approximately 20% (19.55~22.73%). *Sphingobacteria* was the second most dominant, with abundance ranging from 3.29% to 17.72%. Previous studies have shown that some denitrifying bacteria belong to the *Proteobacteria* class [41], indicating a relatively active denitrifying process in all phases. Furthermore, other classes showed more obvious vibration along with the C/N ratio, such as the *Bacteroidia* class, which decreased along with the C/N ratio decrease.

At the family level, *Rhodocyclaceae* is a representative group of aerobic denitrifying bacteria in the wastewater biological treatment process, reducing nitrate to N₂. Its relative abundance increased from 4.21% to 8.88% with the increase in the C/N ratio from 1 to 7 (Figure 8c). This indicated that the increase in C/N can promote the proliferation of *Rhodocyclaceae*, thus improving nitrate removal, which was consistent with the results in Figure 2. The abundance of *Carnobacteriaceae* peaked at 9.29% in the C/N = 5 phase, which was higher than that of C/N = 7. The reason could be that a higher C/N ratio not only

promoted denitrification but also inhibited nitrification. As there was relatively insufficient nitrate/nitrite as the electron acceptors for denitrification, the growth and proliferation of *Carnobacteriaceae* was inhibited [42].

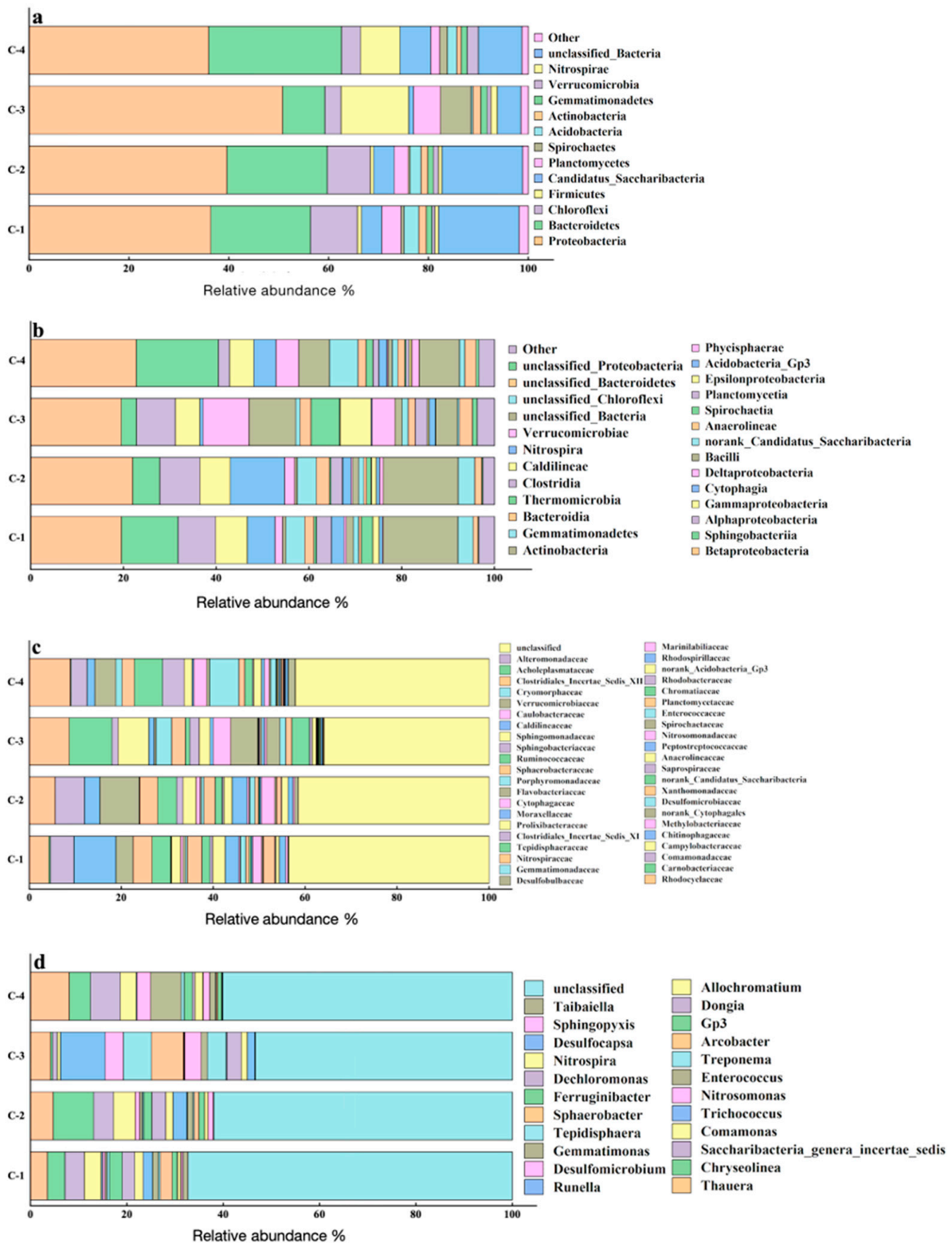


Figure 8. Microbial community changes under different C/N conditions ((a) phylum; (b) class; (c) family; (d) genus).

In Figure 8d, more than 50% of the microbes could not be identified at the genus level. Of the known genera, *Desulfococcus* is found in a variety of wastewater treatment systems as a typical sulfate-reducing bacterium, which generally reduces sulfate to sulfide through desulfurization [43]. In this study, *Desulfococcus*, with a relative abundance of 3.41%, was the dominant group in the C/N = 5 phase. Nitrifying bacteria such as *Nitrosomonas* and *Nitrospira* were present at 3.76% and 1.29% in the C/N = 5 phase, which was higher than the other conditions, and this could explain, to some extent, the higher TN removal efficiency in the C/N = 5 phase (Figure 2). Similarly, the anaerobic denitrifying bacteria *Trichococcus* occupied 9.3% in the C/N = 5 phase, which was much higher than the other phases (0.32% in C/N = 1, 0.021% in C/N = 3, and 0.19% in C/N = 7), indicating that a C/N ratio of 5 was the most suitable for its growth and reproduction.

4. Conclusions

The C/N ratio scarcely affected the COD and NH_4^+ -N removal in the MABR system, with both removal efficiencies around 90~95%. NO_3^- -N accumulated in the C/N = 1 phase until approximately 15 mg/L, and slight NO_2^- -N accumulation was observed in the C/N = 7 phase, leading to lower total nitrogen removal in the two phases. Biomass and biofilm thickness decreased along with the decrease in C/N ratios. EPS generation had a positive correlation to C/N ratios, and the chemical composition was different throughout the phases. Microbial analysis revealed that a C/N ratio of 5 was the most suitable for both nitrifying and denitrifying bacteria, and a higher C/N ratio favored aerobic denitrifying microbes.

Supplementary Materials: The following supporting information can be downloaded at <https://www.mdpi.com/article/10.3390/w15244298/s1>. Figure S1: The set-up of the lab-scale MABR system.

Author Contributions: H.Z.: Investigation, Data Analysis, Writing—original draft; L.D.: Organization, Supervision, Methodology, Writing—Reviewing and Editing; Y.T.: Experiment conduction, Data analysis; L.Q.: Experiment conduction, Writing—original draft; M.W.: Methodology, Writing—Reviewing and Editing. All authors have read and agreed to the published version of the manuscript.

Funding: Huiyun Zhong is supported by Changzhou Leading Innovative Talents Introduction and Cultivation Project (CQ20210117). Liangfei Dong acknowledges the support of the Jiangsu Provincial Ecological Environment Research Project (Achievement Transformation and Promotion Project) (2022013).

Data Availability Statement: Data are contained within the article and supplementary materials.

Conflicts of Interest: The authors declare no conflict of interest.

References

1. Shannon, M.A.; Bohn, P.W.; Elimelech, M.; Georgiadis, J.G.; Mariñas, B.J.; Mayes, A.M. Science and technology for water purification in the coming decades. *Nature* **2008**, *452*, 301–310. [CrossRef] [PubMed]
2. Li, W.; Hai, X.; Han, L.; Mao, J.; Tian, M. Does urbanization intensify regional water scarcity? Evidence and implications from a megaregion of China. *J. Clean. Prod.* **2020**, *244*, 118592. [CrossRef]
3. Solley, D.; Hu, S.; Hertle, C.; Batstone, D.; Karastergiou-Hogan, T.; Rider, Q.; Keller, J. Identifying novel wastewater treatment options through optimal technology integration. *Water Pract. Technol.* **2015**, *10*, 496–504. [CrossRef]
4. Milledge, J.J.; Thompson, E.P.; Sauvêtre, A.; Schroeder, P.; Harvey, P.J. Chapter 8—Novel Developments in Biological Technologies for Wastewater Processing. In *Sustainable Water and Wastewater Processing*; Galanakis, C.M., Agrafioti, E., Eds.; Elsevier: Amsterdam, The Netherlands, 2019; pp. 239–278.
5. Zahoor, M.; Ullah, A.; Alam, S.; Muhammad, M.; Hendroko Setyobudi, R.; Zekker, I.; Sohail, A. Novel Magnetite Nanocomposites ($\text{Fe}_3\text{O}_4/\text{C}$) for Efficient Immobilization of Ciprofloxacin from Aqueous Solutions through Adsorption Pretreatment and Membrane Processes. *Water* **2022**, *14*, 724. [CrossRef]
6. Alam, S.; Khan, M.S.; Umar, A.; Khattak, R.; Rahman, N.U.; Zekker, I.; Burlakovs, J.; Rubins, S.S.D.; Ghangrekar, M.M.; Bhowmick, G.D.; et al. Preparation of Pd–Ni Nanoparticles Supported on Activated Carbon for Efficient Removal of Basic Blue 3 from Water. *Water* **2021**, *13*, 1211. [CrossRef]
7. Nerenberg, R. The membrane-biofilm reactor (MBfR) as a counter-diffusional biofilm process. *Curr. Opin. Biotechnol.* **2016**, *38*, 131–136. [CrossRef] [PubMed]

8. Martin, K.J.; Nerenberg, R. The membrane biofilm reactor (MBfR) for water and wastewater treatment: Principles, applications, and recent developments. *Bioresour. Technol.* **2012**, *122*, 83–94. [[CrossRef](#)]
9. Martin, K.J.; Picioreanu, C.; Nerenberg, R. Multidimensional modeling of biofilm development and fluid dynamics in a hydrogen-based, membrane biofilm reactor (MBfR). *Water Res.* **2013**, *47*, 4739–4751. [[CrossRef](#)]
10. He, H.Q.; Wagner, B.M.; Carlson, A.L.; Yang, C.; Daigger, G.T. Recent progress using membrane aerated biofilm reactors for wastewater treatment. *Water Sci. Technol.* **2021**, *84*, 2131–2157. [[CrossRef](#)]
11. Liu, Y.; Ngo, H.H.; Guo, W.; Peng, L.; Pan, Y.; Guo, J.; Chen, X.; Ni, B.-J. Autotrophic nitrogen removal in membrane-aerated biofilms: Archaeal ammonia oxidation versus bacterial ammonia oxidation. *Chem. Eng. J.* **2016**, *302*, 535–544. [[CrossRef](#)]
12. Kinh, C.T.; Suenaga, T.; Hori, T.; Riya, S.; Hosomi, M.; Smets, B.F.; Terada, A. Counter-diffusion biofilms have lower N₂O emissions than co-diffusion biofilms during simultaneous nitrification and denitrification: Insights from depth-profile analysis. *Water Res.* **2017**, *124*, 363–371. [[CrossRef](#)] [[PubMed](#)]
13. Bunse, P.; Orschler, L.; Agrawal, S.; Lackner, S. Membrane aerated biofilm reactors for mainstream partial nitrification/anammox: Experiences using real municipal wastewater. *Water Res. X* **2020**, *9*, 100066. [[CrossRef](#)] [[PubMed](#)]
14. Chen, R.; Zhou, Y. Measure microbial activity driven oxygen transfer in membrane aerated biofilm reactor from supply side. *Environ. Res.* **2021**, *195*, 110845. [[CrossRef](#)] [[PubMed](#)]
15. Satoh, H.; Ono, H.; Rulin, B.; Kamo, J.; Okabe, S.; Fukushi, K.I. Macroscale and microscale analyses of nitrification and denitrification in biofilms attached on membrane aerated biofilm reactors. *Water Res.* **2004**, *38*, 1633–1641. [[CrossRef](#)] [[PubMed](#)]
16. Semmens, M.J.; Dahm, K.; Shanahan, J.; Christianson, A. COD and nitrogen removal by biofilms growing on gas permeable membranes. *Water Res.* **2003**, *37*, 4343–4350. [[CrossRef](#)] [[PubMed](#)]
17. Gilmore, K.R.; Terada, A.; Smets, B.F.; Love, N.G.; Garland, J.L. Autotrophic Nitrogen Removal in a Membrane-Aerated Biofilm Reactor Under Continuous Aeration: A Demonstration. *Environ. Eng. Sci.* **2013**, *30*, 38–45. [[CrossRef](#)]
18. Downing, L.S.; Nerenberg, R. Total nitrogen removal in a hybrid, membrane-aerated activated sludge process. *Water Res.* **2008**, *42*, 3697–3708. [[CrossRef](#)]
19. Li, M.; Li, P.; Du, C.; Sun, L.; Li, B. Pilot-Scale Study of an Integrated Membrane-Aerated Biofilm Reactor System on Urban River Remediation. *Ind. Eng. Chem. Res.* **2016**, *55*, 8373–8382. [[CrossRef](#)]
20. Seifi, M.; Fazelipour, M.H. Modeling simultaneous nitrification and denitrification (SND) in a fluidized bed biofilm reactor. *Appl. Math. Model.* **2012**, *36*, 5603–5613. [[CrossRef](#)]
21. Pynaert, K.; Smets, B.F.; Beheydt, D.; Verstraete, W. Start-up of Autotrophic Nitrogen Removal Reactors via Sequential Biocatalyst Addition. *Environ. Sci. Technol.* **2004**, *38*, 1228–1235. [[CrossRef](#)]
22. Sun, Z.; Li, Y.; Yue, J.; Song, Z.; Li, M.; Wang, N.; Liu, J.; Guo, H.; Li, B. Metagenomic analysis revealed the mechanism of extracellular polymeric substances on enhanced nitrogen removal in coupled MABR systems with low C/N ratio containing salinity. *J. Environ. Chem. Eng.* **2023**, *11*, 109599. [[CrossRef](#)]
23. Ding, S.; He, J.; Luo, X.; Zheng, Z. Simultaneous nitrogen and carbon removal in a packed A/O reactor: Effect of C/N ratio on microbial community structure. *Bioprocess Biosyst. Eng.* **2020**, *43*, 1241–1252. [[CrossRef](#)] [[PubMed](#)]
24. Tong, Y.; Wang, M.; Peñuelas, J.; Liu, X.; Paerl, H.W.; Elser, J.J.; Sardans, J.; Couture, R.-M.; Larssen, T.; Hu, H.; et al. Improvement in municipal wastewater treatment alters lake nitrogen to phosphorus ratios in populated regions. *Proc. Natl. Acad. Sci. USA* **2020**, *117*, 11566–11572. [[CrossRef](#)] [[PubMed](#)]
25. Abdelfattah, A.; Eltawab, R.; Iqbal Hossain, M.; Zhou, X.; Cheng, L. Membrane aerated biofilm reactor system driven by pure oxygen for wastewater treatment. *Bioresour. Technol.* **2024**, *393*, 130130. [[CrossRef](#)] [[PubMed](#)]
26. Zhang, C.; Quan, B.; Tang, J.; Cheng, K.; Tang, Y.; Shen, W.; Su, P.; Zhang, C. China's wastewater treatment: Status quo and sustainability perspectives. *J. Water Process Eng.* **2023**, *53*, 103708. [[CrossRef](#)]
27. APHA. *Standard Methods for the Examination of Water and Wastewater*, 19th ed.; American Public Health Association: Washington, DC, USA, 1995.
28. Celmer, D.; Oleszkiewicz, J.A.; Cicek, N. Impact of shear force on the biofilm structure and performance of a membrane biofilm reactor for tertiary hydrogen-driven denitrification of municipal wastewater. *Water Res.* **2008**, *42*, 3057–3065. [[CrossRef](#)] [[PubMed](#)]
29. More, T.T.; Yadav, J.S.S.; Yan, S.; Tyagi, R.D.; Surampalli, R.Y. Extracellular polymeric substances of bacteria and their potential environmental applications. *J. Environ. Manag.* **2014**, *144*, 1–25. [[CrossRef](#)]
30. Lai, C.-Y.; Dong, Q.-Y.; Chen, J.-X.; Zhu, Q.-S.; Yang, X.; Chen, W.-D.; Zhao, H.-P.; Zhu, L. Role of Extracellular Polymeric Substances in a Methane Based Membrane Biofilm Reactor Reducing Vanadate. *Environ. Sci. Technol.* **2018**, *52*, 10680–10688. [[CrossRef](#)]
31. Herbert, D.; Phipps, P.J.; Strange, R.E. Chapter III Chemical Analysis of Microbial Cells. In *Methods in Microbiology*; Norris, J.R., Ribbons, D.W., Eds.; Academic Press: Cambridge, MA, USA, 1971; pp. 209–344.
32. Pierce, J.; Suelter, C.H. An evaluation of the Coomassie brilliant blue G-250 dye-binding method for quantitative protein determination. *Anal. Biochem.* **1977**, *81*, 478–480. [[CrossRef](#)]
33. Rajakaruna, H.; Drake, A.R.; Chan, F.T.; Bailey, S.A. Optimizing performance of nonparametric species richness estimators under constrained sampling. *Ecol. Evol.* **2016**, *6*, 7311–7322. [[CrossRef](#)]
34. Lin, J.; Zhang, P.; Li, G.; Yin, J.; Li, J.; Zhao, X. Effect of COD/N ratio on nitrogen removal in a membrane-aerated biofilm reactor. *Int. Biodeterior. Biodegrad.* **2016**, *113*, 74–79. [[CrossRef](#)]

35. Matsumoto, S.; Terada, A.; Tsuneda, S. Modeling of membrane-aerated biofilm: Effects of C/N ratio, biofilm thickness and surface loading of oxygen on feasibility of simultaneous nitrification and denitrification. *Biochem. Eng. J.* **2007**, *37*, 98–107. [[CrossRef](#)]
36. Zhang, B.; Guo, Y.; Lens, P.N.; Zhang, Z.; Shi, W.; Cui, F.; Tay, J.H. Effect of light intensity on the characteristics of algal-bacterial granular sludge and the role of N-acyl-homoserine lactone in the granulation. *Sci. Total Environ.* **2019**, *659*, 372–383. [[CrossRef](#)] [[PubMed](#)]
37. Zhu, L.; Qi, H.-Y.; Lv, M.-L.; Kong, Y.; Yu, Y.-W.; Xu, X.-Y. Component analysis of extracellular polymeric substances (EPS) during aerobic sludge granulation using FTIR and 3D-EEM technologies. *Bioresour. Technol.* **2012**, *124*, 455–459. [[CrossRef](#)] [[PubMed](#)]
38. Wong, M.K.-S.; Nakao, M.; Hyodo, S. Field application of an improved protocol for environmental DNA extraction, purification, and measurement using Sterivex filter. *Sci. Rep.* **2020**, *10*, 21531. [[CrossRef](#)] [[PubMed](#)]
39. Jolliffe, I.T.; Cadima, J. Principal component analysis: A review and recent developments. *Philos. Trans. A Math. Phys. Eng. Sci.* **2016**, *374*, 20150202. [[CrossRef](#)]
40. Fang, D.; Zhao, G.; Xu, X.; Zhang, Q.; Shen, Q.; Fang, Z.; Huang, L.; Ji, F. Microbial community structures and functions of wastewater treatment systems in plateau and cold regions. *Bioresour. Technol.* **2018**, *249*, 684–693. [[CrossRef](#)]
41. Heylen, K.; Vanparys, B.; Wittebolle, L.; Verstraete, W.; Boon, N.; De Vos, P. Cultivation of denitrifying bacteria: Optimization of isolation conditions and diversity study. *Appl. Environ. Microbiol.* **2006**, *72*, 2637–2643. [[CrossRef](#)]
42. Qian, G.; Li, L.; Hu, X.; Yu, X.; Ye, L. Enhancement of the biodegradability of activated sludge by the electric-coagulation multistage A/O membrane bioreactor treating low C/N industrial wastewater. *Int. Biodeterior. Biodegrad.* **2017**, *125*, 1–12. [[CrossRef](#)]
43. Guo, J.; Li, Y.; Sun, J.; Sun, R.; Zhou, S.; Duan, J.; Feng, W.; Liu, G.; Jiang, F. pH-dependent biological sulfidogenic processes for metal-laden wastewater treatment: Sulfate reduction or sulfur reduction? *Water Res.* **2021**, *204*, 117628. [[CrossRef](#)]

Disclaimer/Publisher’s Note: The statements, opinions and data contained in all publications are solely those of the individual author(s) and contributor(s) and not of MDPI and/or the editor(s). MDPI and/or the editor(s) disclaim responsibility for any injury to people or property resulting from any ideas, methods, instructions or products referred to in the content.